SAND2017-13267J

A comparison of control strategies for wave energy converters

Ryan G. Coe[a,*], Giorgio Bacelli[a], David G. Wilson[a], Ossama Abdelkhalik[b], Umesh A. Korde[b], Rush D. Robinett III[b]

[a]*Sandia National Labs, P.O. BOX 5800 MS 1124, Albuquerque, NM 87106, USA*
[b]*Michigan Technological University, 1400 Townsend Drive, Houghton, MI 49931-1295, USA*

Abstract

In this study, we employ a numerical model to compare the performance of a number of wave energy converter control strategies. The controllers selected for evaluation span a wide range in their requirements for implementation. Each control strategy is evaluated using a single numerical model with a set of sea states to represent a deployment site off the coast of Newport, OR. A number of metrics, ranging from power absorption to kinematics, are employed to provide a comparison of each control strategy's performance that accounts for both relative benefits and costs. The results show a wide range of performances from the different controllers and highlight the need for a holistic design approach which considers control design as a parallel component within the larger process WEC design.

Keywords: wave energy, control, dynamics

1. Introduction

The energy contained in ocean waves is distributed across a wide range of frequencies. In order to produce electricity efficiently, wave energy converters (WECs) must be designed to capture a large share of the energy from a broad range of ocean wave frequencies. Additionally, the majority of energy in ocean waves exists at relatively low frequencies, which are most easily accessed by relatively large WECs. To limit the size, and therefore cost, of a WEC and to increase energy absorption over a broad range of frequencies, an increasing body of research has shown power take-off (PTO) control to be an attractive path.

*rcoe@sandia.gov

The dynamic system of a WEC can be considered as a series of subsystems. A hydrodynamic/hydrostatic process transfers energy from the ocean to the WEC device; a mechanical process transfers energy from the moving bodies of the WEC to PTO; a hydraulic/magnetic/electrical process transfers the mechanical energy to electricity. Considering the wide range of WECs currently under design, this coupled system can take many forms. While this description vastly over simplifies the various physical processes involved, it does begin to emphasize the multi-layer nature of the system of interest. The hydrodynamic/hydrostatic and mechanical properties of WEC can produce a certain frequency response; however, when coupled with input from a PTO, which can be understood to act as some combination of a spring, a damper, and a mass, a new frequency response for the overall device is achieved. It is on this basis that specific control strategies for WEC PTOs can influence energy absorption.

A large range of strategies have been proposed and studied for the control of a WEC PTO. Budal and Falnes considered both reactive control and latching in the early 1970s and carried out much of the early development of latching-type 'phase control' through both theory and wave tank experimentation [1]. An independent early application of this approach was recorded in the U.S. by Dedger Jones [2]. Latching control was soon being studied for WEC control by a number of other groups around the world (see, e.g., [3, 4, 5, 6]). Scruggs et al. applied a linear quadratic Gaussian (LQG) control, which incorporates spectrally-dependent gain parameters [7]. Many studies in the past two decades have also considered model predictive control (MPC) for WECs [8, 9]. Hals et al. studied a series of control strategies and provided some comparison of these options [10].

This study presents eight different control strategies for WEC control. Individual controller implementations are presented and discussed. These strategies are implemented for a single case study WEC device, and are used to run a series of numerical simulations. From these simulations, we compare results to better understand the relative performance of these different control strategies, in addition to the PTO characteristics required to implement each of the algorithm. We conclude the study with some discussion on the various trade-offs between these different approaches.

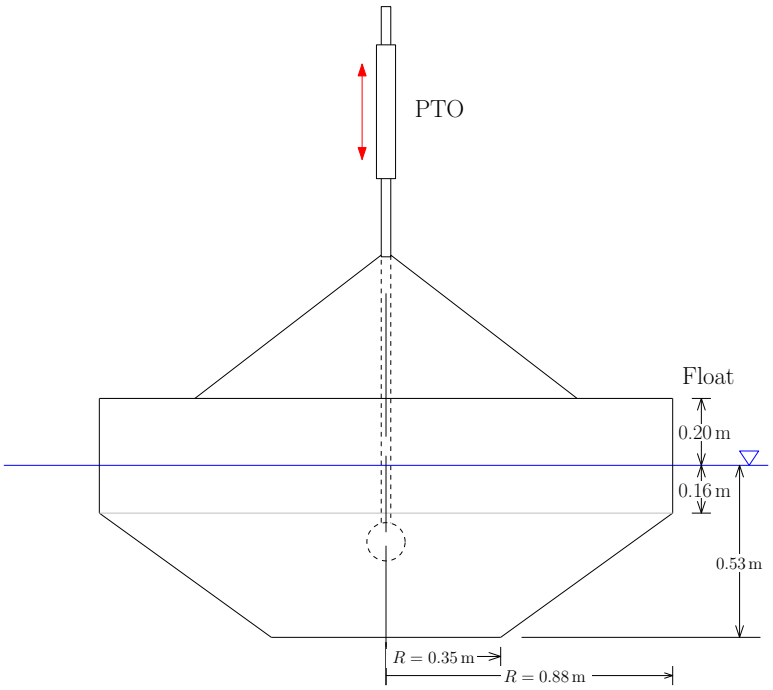

Figure 1: Test-bed WEC device used for control comparison.

2. Background

2.1. Study device

A test-bed WEC device was designed with the purpose of evaluating system identification, modeling, and control approaches [11]. Figure 1 shows an illustration of this device, highlighting the waterline, draft and key dimensions. This device is designed to allow motion in 3 degrees-of-freedom (DOF), however, for this study only motion in heave is considered. A list of the relevant physical parameters for this WEC are listed in Table 1. This device is considered to be roughly 1/20th-scale when compared with current designs for grid-scale systems.

2.2. Numerical model

A model for the heave velocity of the device introduced in Section 2.1 has been developed using the formulation of Cummins [12]. In the time domain, the heave velocity

Table 1: Model-scale WEC physical parameters.

Parameter	Value
Rigid-body mass (float & slider), m (kg)	858
Displaced volume, $\forall$ (m^3)	0.858
Float radius, r (m)	0.88
Float draft, T (m)	0.53
Water density, ρ (kg/m^3)	1000

can be described by the Volterra integro-differential equation [13]

$$(m + A_\infty)\ddot{z} + \int_0^t k_r(t-\lambda)\dot{z}\,(\lambda)\; d\lambda + b_v\dot{z} + k_{hs}z = f_e(t) + f_u(t), \tag{1}$$

where z is the vertical position of the device. The rigid-body and hydrodynamic infinite-frequency added mass are represented by m and A_∞, respectively. Radiation damping and frequency-dependent added mass are incorporated via the impulse response function k_r. The linear product $b_v\dot{z}$ accounts for viscous damping effects. The hydrostatic/gravitational spring contribution is given by k_{hs}.

$$k_{hs} = \rho g A_{wp} \tag{2}$$

Here, A_{wp} is the area of the water plane. The density of the water and gravitational constant are ρ and g, respectively.

The force applied by the PTO is represented by f_u, which is dependent on the control strategy imposed. Wave excitation forces are represented by f_e. By working in the frequency domain, these can be obtained for some complex wave spectrum by taking the complex product of the wave input, $\zeta(\omega)$, and the device's excitation frequency response function (FRF), $H(\omega)$, as:

$$F_e(\omega) = H(\omega)\zeta(\omega). \tag{3}$$

Thus, $F_e(\omega)$ is the complex excitation, which can be used to obtain a the time history of excitation, $f_e(t)$, via the inverse Fourier transform.

The convolution term in (1) can be replaced by fitting a parametric model to the radiation FRF (see, e.g., [14, 15]). In state-space form, this can be written as

$$\begin{aligned} \dot{x}_r &= A_r x_r + B_r \dot{z}(t) \\ \breve{\mu}(t) &= C_r x_r, \end{aligned} \tag{4}$$

Here, A_r, B_r, and C_r are the radiation state, input and output matrices, respectively. Similarly, radiation states are stored via x_r. The matrices A_r, B_r, and C_r can be tuned to approximate the non-parametric radiation FRF in either the time or frequency domain. Applying (4) along with some minor manipulations, we can rewrite (1) as system of first order ordinary differential equations (ODEs).

$$\begin{aligned} \dot{z} &= v \\ (m + A_\infty)\dot{v} &= -C_r x_r - b_v v - k_{hs} z + f_e(t) + f_u(t) \\ \dot{x}_r &= A_r x_r + B_r \dot{z}(t) \end{aligned} \tag{5}$$

Using (5), we can rewrite the dynamic equation for the vertical velocity of the WEC as a single state-space model.

$$\begin{aligned} \dot{\mathbf{x}}_c(t) &= A_c \mathbf{x}_c + B_c(u_c(t) + v_c(t)) \\ \mathbf{y}_c(t) &= C_c \mathbf{x}_c(t) \end{aligned} \tag{6}$$

Here, $u_c(t)$ and $v_c(t)$ are control input and excitation, respectively. The state variable $\mathbf{x}_c$ and the output variable $\mathbf{y}_c$ are defined, respectively, as

$$\mathbf{x}_c = \begin{bmatrix} z \\ v \\ \mathbf{x}_r \end{bmatrix} \in \mathbb{R}^{2+n} \qquad \mathbf{y}_c = \begin{bmatrix} z \\ v \end{bmatrix} \in \mathbb{R}^2. \tag{7}$$

The matrices A_c, B_c and C_c are

$$A_c = \begin{bmatrix} 0 & 1 & \mathbf{0} \\ \frac{-k_h}{m+A_\infty} & \frac{-b_v}{m+A_\infty} & \frac{-1}{m+A_\infty} C_r \\ \mathbf{0} & B_r & A_r \end{bmatrix} \in \mathbb{R}^{(n+2)\times(n+2)} \tag{8}$$

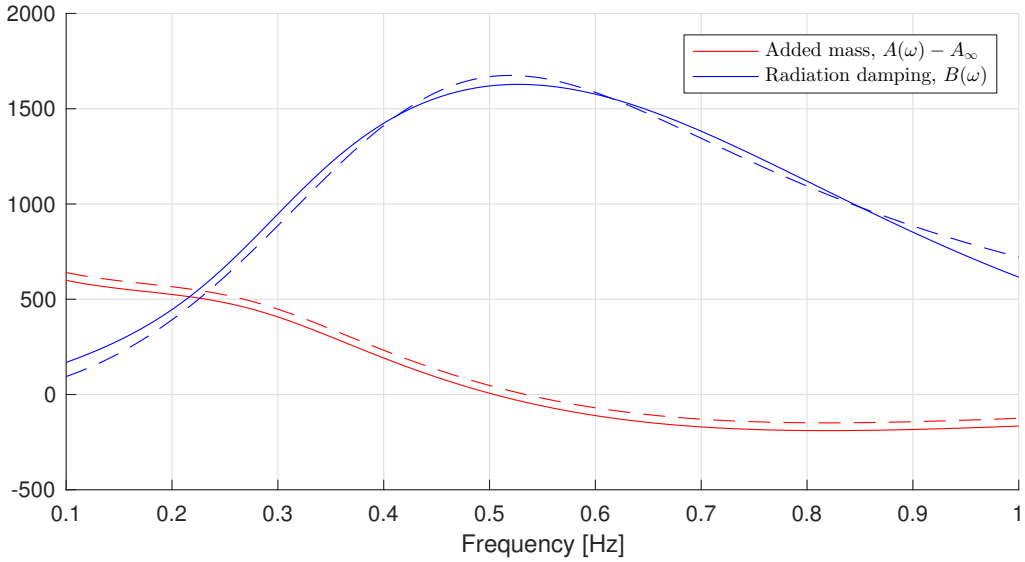

Figure 2: Added mass and radiation damping frequency response functions for WEC device; WAMIT in solid lines (-), experiment in dashed lines (- -).

$$B_c = \begin{bmatrix} 0 \\ \frac{1}{m+A_\infty} \\ \mathbf{0} \end{bmatrix} \in \mathbb{R}^{(n+2)\times 1}, \qquad C_c = \begin{bmatrix} 1 & 0 & \mathbf{0} \\ 0 & 1 & \mathbf{0} \end{bmatrix} \in \mathbb{R}^{2\times(n+2)}. \tag{9}$$

An initial version of this model employed coefficients obtained from the boundary element (BEM) tool WAMIT [16]. Data collected during experimental wave tank testing showed good agreement with this model [17]. The added mass and radiation damping FRFs from both of these cases (numerical and experimental) are shown in Figure 2. The FRFs from WAMIT are shown with solid lines; the FRFs based on empirical testing and system identification are shown with dashed lines.

2.3. Study environment

A deployment climate of Newport, OR is considered for the comparisons performed in this study. A joint probability distribution (JPD) is used to assign probabilities of a finite set of sea states. Using a k-means clustering approach (see, e.g., [18]), a set of 17 Bretschneider sea states were selected to represent the deployment climate. All 17 of the sea states considered for this study are shown in Figure 3 and listed in Table 2.

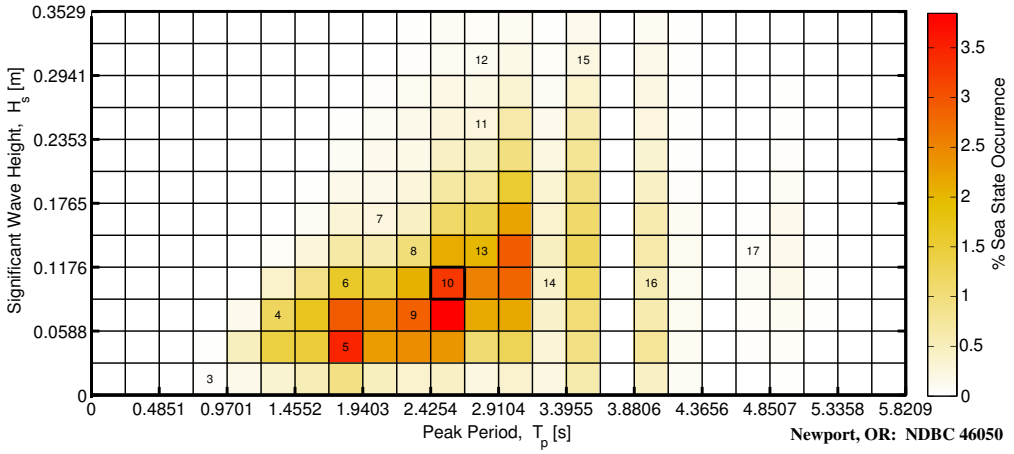

Figure 3: Numbering of the sea state. NOTE: sea states 1, 2, and 3 all fall in the same bin.

Here, the probability distribution of the Newport, OR climate is shown via shading in the background and the indexing number of each sea state identified in Table 2 is associated with the corresponding bin in the JPD.

3. Control strategies

The main purpose of a controller is to alter the dynamic behavior of a given system (in this case a WEC) in order to pursue a specific objective (e.g., maximize power absorption, smooth power output, limit loads). The majority of power produced by WEC devices occurs during resonant absorption, when the excitation force is in phase with device velocity. Thus, the control strategies considered in this study, which foremost consider maximizing power absorption, generally attempt to alter the system dynamics in order to achieve resonance.

Figure 4 depicts a generalized structure of a control system applied, in this particular case, to a WEC (shown as $G(s)$ in Figure 4). In general, the architecture of a control system is composed of two main blocks: feedback (FB) and feedforward (FF). The name feedback derives from the fact that an output signal (or a set of output signals), marked as y in Figure 4, is measured and fed back to the control system which continuously reacts, based on the current and past measurements, according to the control objective. Conversely, a controller implemented in feedforward mode generates a control signal

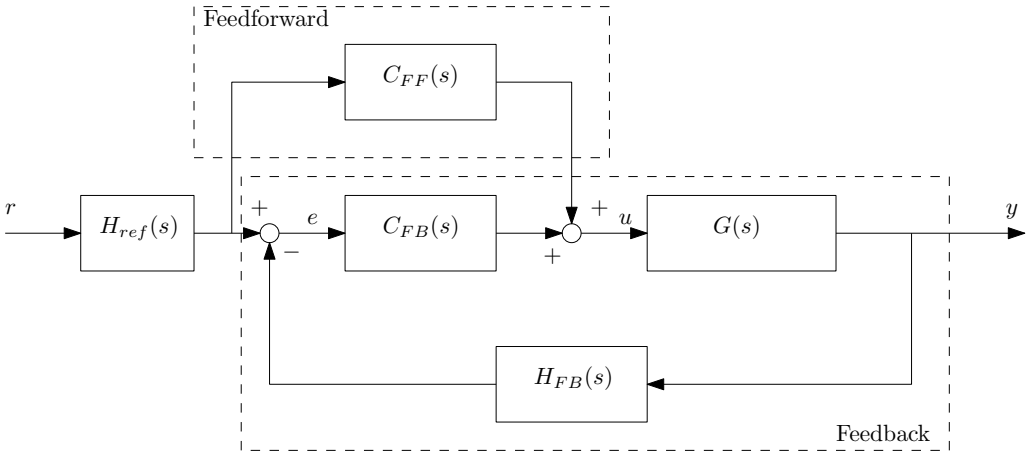

Figure 4: Basic feedforward/feedback controller structure [20].

based on a reference (r in Figure 4) which can be pre-determined or calculated from some quantities not related to the state of the system (e.g., incident wave elevation). Pure feedforward controllers do not react to the instantaneous state of the system (no signal is fed back to the controller). In practice, it is common for control systems to be built by combining both feedback and feedforward. The design of the control system consists of developing the control functions (FF and FB), by using the controller model, with respect to some desired performance objective. Figure 4 also depicts a pre-filter block, denoted by H_{ref}, that can be used to improve the properties of the closed-loop system, such as stability margins and sensitivity to noise and parameter uncertainty (modeling errors). This type of structure is generally known as a two degrees of freedom controller [19].

A number of control strategies considered here employ optimization algorithms. Optimization can be used in both the design of a control strategy (i.e., to determine some optimal gain factors) and/or in the during execution to determine the control signal. Linear quadratic control (LQ; Section 3.6) and a proportional-derivative version of complex conjugate Control (PDC3; Section 3.7) employ optimization in control design. Model predictive control (MPC; Section 3.3), shape based control (SB; Section 3.5), and dynamic programming (DP; Section 3.3) employ optimization during execution to determine the control signal. This process often follows a receding horizon structure, as depicted in

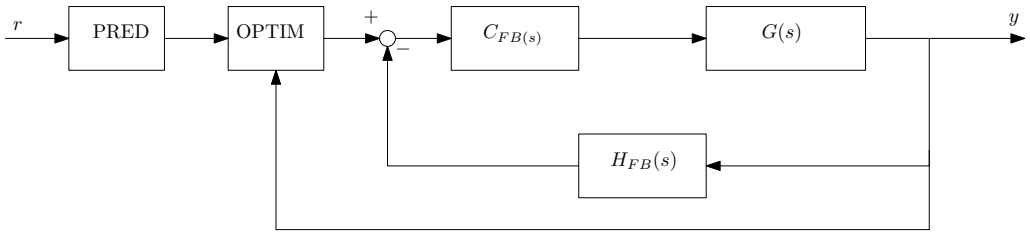

Figure 5: Basic structure for "receding horizon."

Figure 5. Here, a control decision is computed based on predictions over a some finite future time. The current system state is measured and used as initial conditions at each time step in the controller computation. In some cases (such as DP and SB) the computational resources required for optimization can limit real-time implementation. While these methods may not be implemented for real-time execution, they can still provide valuable insights for the control design process.

The following sections describe eight different control strategies which are considered and implemented here for the control of the WEC introduced in Section 2.1. Some of the strategies require reactive power, while others do not. Similarly, certain strategies are better suited than others to incorporating constraints. As shown in Table 3, the strategies selected here span the design space. Note that in some cases, a given control strategy may be implemented in a number a ways; the categorization in Table 3 reflects the most standard implementation of each strategy and that which is considered in the present study. For example, while Table 3 records the possibility of including constraints for a number of control strategies, no constraints were included in this study except for when necessary to enforce stability. Similarly, Table 3 shows that MPC, DP, SB require reactive power. However, since constraints can be introduced to these strategies, it is possible to limit the power to be one-side (i.e., no reactive power). The computational expense presented in Table 3 was determined based on the simulations run for this study. Another factor which should be considered is that the different strategies are inherently at different levels of implementation. For example, DP is considered primarily as a design tool, and due to high computational expense would be very challenging to implement on a real-time system. At the other end of the spectrum, LQ is readily implementable on a real-time system and even uses a simple model of PTO efficiency.

3.1. Resistive control

In resistive damping control, a constant of proportionality between the force and velocity determines the resistance offered, which is also the power absorption rate. Net power capture from a wave-excited oscillating body is a resistive process. Therefore, this control strategy is a simple proportional feedback.

$$f_u = -b_{PTO}\, v \tag{10}$$

Here, the constant damping factor is b_{PTO} and serves as the proportional gain. Optimal values of b_{PTO} can be determined analytically (assuming potential flow) for monochromatic waves (see, e.g., [21]). For irregular sea states, numerical optimization can be applied.

3.2. Complex conjugate control (CCC)

As resistive control is considered somewhat of a lower bounding case for gross WEC energy absorption, complex conjugate control (CCC) is considered to represent an upper bound. Working in the frequency domain, we can rewrite (1) as

$$\left(i\omega\left(m + A(\omega)\right) + B(\omega) + b_v + \frac{k_{hs}}{i\omega}\right) V(\omega) = F_e(\omega) + F_u(\omega). \tag{11}$$

From the left hand side of (11), we can define the intrinsic impedance (see, e.g., [21]) for the WEC as

$$Z_i(\omega) = i\omega\left(m + A(\omega)\right) + B(\omega) + b_v + \frac{k_{hs}}{i\omega}, \tag{12}$$

such that

$$\begin{aligned} Z_i(\omega)V(\omega) &= F_e(\omega) + F_u(\omega) \\ &= F_{\text{ext}}(\omega). \end{aligned} \tag{13}$$

Solving for the complex velocity $V(\omega)$, we have

$$V(\omega) = \frac{F_{\text{ext}}(\omega)}{Z_i(\omega)} = \frac{F_{\text{ext}}(\omega)}{\left(i\omega\left(m + A(\omega)\right) + B(\omega) + b_v + \frac{k_{hs}}{i\omega}\right)}. \tag{14}$$

If we define some impedance, $Z_u(\omega)$ for the PTO force, such at $F_u(\omega) = -Z_u(\omega)V(\omega)$, the useful time-averaged power produced will subsequently be

$$\begin{aligned} P_u(\omega) &= \frac{1}{2}\mathbb{R}\left\{-F_u(\omega)\dot{z}(\omega))\right\} \\ &= \frac{1}{2}\mathbb{R}\left\{Z_u(\omega)\right\}\left|\dot{z}(\omega)\right|^2 \end{aligned}. \tag{15}$$

For resonance, it can be shown that maximum useful power is obtained by setting

$$Z_u(\omega) = -Z_i^*(\omega), \tag{16}$$

where * denotes the complex conjugate.

It is well known that when $F_e(\omega)$ is formed as function of the wave elevation at the location of the floating body (as is typical), (16) is non-causal (i.e., $f_u(t)$ depends on future values of $f_e(t)$) [22]. For this study, as described in Section 2.2, we simply pre-compute $f_e(t)$ for the entire simulation period. This represents an assumption of perfect prediction of incoming waves (as well as the location of the device). The control strategies that depend on current and future knowledge of the excitation force (i.e., CCC, MPC, DP, SB) will undoubtedly benefit from this assumption. Thus, this assumption leads to an upper estimate for the performance of these strategies.

3.3. Model predictive control (MPC)

Model predictive control is an optimization based control strategy that is derived from attempting to solve a quadratic programing (QP) problem in a receding horizon fashion (see Figure 5). In the implementation employed here, no inner feedback loop has been considered, therefore the transfer function of the feedback block is $H_{FB}(s) = 0$ and the controller is $C_{FB}(s) = 1$, however, as shown in Figure 5, the current state of the system is passed to the optimization block directly. The signal r is the excitation force and the prediction block ("PRED" in Figure 5) predicts the value of the excitation force over some time horizon, which is used to optimize the PTO input. As noted in Section 3.2, for this study the prediction process is assumed to be perfect. The receding horizon procedure is repeated iteratively to compensate for disturbances and imperfect modeling by updating the current state of the system every time the optimization is carried out.

The MPC algorithm requires the dynamic model to be formulated in discrete time. Following [8], the discretization of the model in (6) is carried out by means of a triangle-hold (first order-hold), which results in continuous and piecewise linear profile for the optimal PTO force. The benefit of this type of discretization is to allow for a longer update interval compared to a zero-hold discretization, which provides only a discontinuous, piecewise constant profile for the optimal control force. Thus, the state space model resulting from the discretization is

$$\mathbf{x}(k+1) = A\,\mathbf{x}(k) + B\,\Delta u(k+1) + F\,\Delta v(k+1) \tag{17}$$

$$\mathbf{y}(k) = C\,\mathbf{x}(k). \tag{18}$$

Here, the matrices A, B, F, and C are

$$A = \begin{bmatrix} \phi(h) & \Gamma & \Gamma \\ 0 & 1 & 0 \\ 0 & 0 & 1 \end{bmatrix} \in \mathbb{R}^{(n+4)\times(n+4)} \qquad B = \begin{bmatrix} \Lambda \\ 1 \\ 0 \end{bmatrix} \in \mathbb{R}^{(n+4)\times 1} \tag{19}$$

$$F = \begin{bmatrix} \Lambda \\ 0 \\ 1 \end{bmatrix} \in \mathbb{R}^{(n+4)\times 1} \qquad C = \begin{bmatrix} 1 & 0 & 0 & \dots & 0 & 0 & 0 \\ 0 & 1 & 0 & \dots & 0 & 0 & 0 \\ 0 & 0 & 1 & \dots & 0 & 0 & 0 \end{bmatrix} \in \mathbb{R}^{3\times(n+4)}, \tag{20}$$

with $\phi(h) = e^{A_c\,h}$ and

$$\Gamma = A_c^{-1}\left(\phi(h) - I\right)\,B_c \;\in \mathbb{R}^{(n+2)\times 1} \tag{21}$$

$$\Lambda = \frac{1}{h} A_c^{-1}\left(\Gamma - h\,B_c\right) \quad \in \mathbb{R}^{(n+2)\times 1}. \tag{22}$$

Note that the state vector, $\mathbf{x}(k)$, has been augmented by including the PTO force and the excitation force; also the output vector has been augmented to include the PTO force. The state and output vectors have been augmented because the input has been expressed as increments with respect to its previous value (Δu and Δv are the change in control input and excitation, respectively), therefore the dynamical system had to be augmented with two integrators corresponding to the last two rows of matrix A.

Letting N denote the number of prediction steps, the predicted output of the system can be written as function of the current state and future inputs increments as

$$\underline{\mathbf{y}}(k) = \mathcal{P}\mathbf{x}(k) + \mathcal{T}_u \underline{\Delta \mathbf{u}}(k) + \mathcal{T}_v \underline{\Delta \mathbf{v}}(k), \tag{23}$$

where $\mathcal{P}$, $\mathcal{T}_u$ and $\mathcal{T}_v$ are

$$\mathcal{P} = \begin{bmatrix} C\,A \\ C\,A^2 \\ \vdots \\ C\,A^N \end{bmatrix} \in \mathbb{R}^{3N\times(n+4)} \tag{24}$$

$$\mathcal{T}_u = \begin{bmatrix} C\,B & 0 & 0 & \dots \\ C\,A\,B & C\,B & 0 & \dots \\ C\,A^2\,B & C\,A\,B & C\,B & \dots \\ \vdots & \vdots & \vdots & \vdots \\ C\,A^{N-1}\,B & C\,A^{N-2}\,B & C\,A^{N-3}\,B & \dots \end{bmatrix} \in \mathbb{R}^{3N\times N} \tag{25}$$

$$\mathcal{T}_v = \begin{bmatrix} C\,F & 0 & 0 & \dots \\ C\,A\,F & C\,F & 0 & \dots \\ C\,A^2\,F & C\,A\,F & C\,F & \dots \\ \vdots & \vdots & \vdots & \vdots \\ C\,A^{N-1}\,F & C\,A^{N-2}\,F & C\,A^{N-3}\,F & \dots \end{bmatrix} \in \mathbb{R}^{3N\times N} \tag{26}$$

The quantity to be maximized is the mechanical work done by the PTO over the prediction horizon T, expressed as

$$E_{t,t+T} = -(m + A_\infty) \int_t^{t+T} u(\tau) v(\tau)\, d\tau. \tag{27}$$

By means of the discretization, this quantity can be written in matrix form as the quadratic cost function J

$$J = \frac{1}{2} \underline{\Delta \mathbf{u}}^T \mathcal{T}_u^T Q \mathcal{T}_u \underline{\Delta \mathbf{u}} + \underline{\Delta \mathbf{u}}^T \mathcal{T}_u^T Q \left(\mathcal{P}\mathbf{x} + \mathcal{T}_v \underline{\Delta \mathbf{v}}\right), \tag{28}$$

where Q and M are

$$Q = \begin{bmatrix} M & & & \\ & \ddots & & \\ & & M & \\ & & & \frac{1}{2}M \end{bmatrix}, \qquad M = \begin{bmatrix} 0 & 0 & 0 \\ 0 & 0 & 1 \\ 0 & 1 & 0 \end{bmatrix}. \tag{29}$$

Constraints on the maximum PTO force and maximum displacement can be included in the formulation of the optimization problem using the linear inequalities

$$\begin{bmatrix} M_z \\ -M_z \end{bmatrix} \mathcal{T}_u \underline{\Delta \mathbf{u}} = \begin{bmatrix} -M_z \\ M_z \end{bmatrix} (\mathcal{P}\mathbf{x} + \mathcal{T}_v \underline{\Delta \mathbf{v}}) + z_{max} \tag{30}$$

$$\begin{bmatrix} M_f \\ -M_f \end{bmatrix} \mathcal{T}_u \underline{\Delta \mathbf{u}} = \begin{bmatrix} -M_f \\ M_f \end{bmatrix} (\mathcal{P}\mathbf{x} + \mathcal{T}_v \underline{\Delta \mathbf{v}}) + f_{max}, \tag{31}$$

where M_z and M_f are

$$M_z = \begin{bmatrix} C_z & & & \\ & \ddots & & \\ & & C_z & \\ & & & C_z \end{bmatrix} \in \mathbb{R}^{N \times 3N} \quad C_z = [1\ 0\ 0] \tag{32}$$

$$M_f = \begin{bmatrix} C_f & & & \\ & \ddots & & \\ & & C_f & \\ & & & C_f \end{bmatrix} \in \mathbb{R}^{N \times 3N} \quad C_f = [0\ 0\ 1]. \tag{33}$$

3.4. Dynamic programming (DP)

Dynamic programming (DP) is a useful mathematical technique for making a sequence of interrelated decisions. It provides a systematic procedure for determining the optimal combination of decisions [23]. The basis of the DP approach is the Bellman's principle of optimality [24]. An optimal sequence of decisions has the property that at any stage (time) the remaining decisions must be optimal for the remaining problem

with the decision and state resulting from the previous decision considered as initial conditions. There is no standard mathematical formulation of the dynamic programming problem; unlike other techniques, such as linear programming, DP is a general approach to problem solving.

Hence the implementation of DP requires developing a tailored algorithm and equations for the particular application. In this optimal WEC control problem, the space-time domain is discretized. This discretization renders the obtained solution sub-optimal. At each time node, the problem can be thought of as searching for the optimal control (decision) at that time, such that the extracted energy is maximized over a given future horizon. DP is a receding horizon strategy (see Figure 5) and in the current implementation does not include a inner feedback loop (block $C_{FB}(s) = 1$ and feedback block $H_{FB}(s) = 0$). Instead, as shown in Figure 5, the current state of the system is passed to the optimization block directly.

The states are discretized in space and time. This discretization is fundamental for DP operation and is crucial for computational efficiency/feasibility of the DP approach. Given maximum and minimum values for each of the system states, the state space is divided into nodes of equal inter-spaces. The number of nodes for the states, $N_{x1}, N_{x2}, \cdots, N_{xn}$, are tuning parameters. An illustration for a two-dimensional discretized domain is shown in Figure 6. In this discretized domain, any state $\vec{x}_i$, for instance in box 1, is associated with the state vector at the node $\vec{x}_{\mathbf{a}l}$ in the same box. When the system transitions from a state $\vec{x}_i$ at time step k to a state $\vec{x}_j$, for instance in box 2, at time step $k+1$ through a control u, the two associated states for $\vec{x}_i$ and $\vec{x}_j$, $\vec{x}_{\mathbf{a}l}$ and $\vec{x}_{\mathbf{a}m}$, respectively, are computed and stored. The transition between any two other states whose associated states are also $\vec{x}_{\mathbf{a}l}$ and $\vec{x}_{\mathbf{a}m}$ (i.e., transition between any state in box 1 to any state in box 2) at the time step k and $k+1$, respectively, is considered to have the same fitness value as the fitness of the transition between $\vec{x}_i$ and $\vec{x}_j$; hence a significant computational effort can be saved.

The process of dynamic programming for the WEC optimal control is here described. Suppose that the control is updated at a rate of u_{rate} Hz. Given a current state vector $\vec{x}_k$ and current time t_k, the optimal control over a horizon (H seconds) is computed, $u_1, u_2, \ldots u_N$, where $N = H \times u_{rate}$. Only the first control u_1 is used to update the

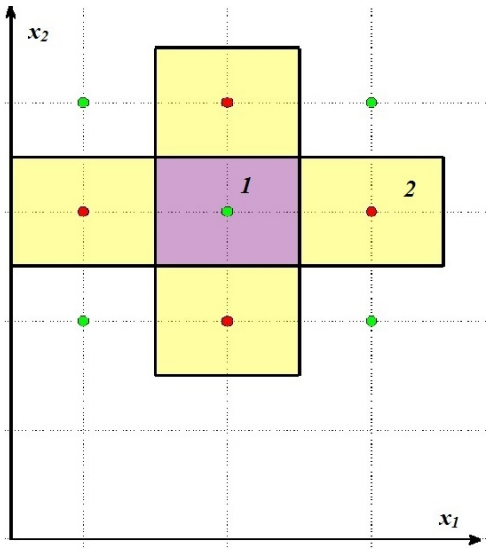

Figure 6: Discretization of the state space for DP implementation.

current state to a new state $\vec{x}_{k+1}$. This process is repeated. To implement this process, three matrices are constructed and updated at a rate u_{rate}; also an index is given to each associated state. The three matrices are: $S_{Ind,N}$, $U_{Ind,N}$, and $I_{Ind,N}$, where $Ind = N_{x1} \times N_{x2}$ is the total number of indices. The matrix $S_{Ind,N}$ contains associated states at N different times starting from the current time until the end of the horizon H. The matrix element $S(i,k)$, for instance, includes the index of the associated states at time $k-1$ that is transitioned to the associated state i at time k. The corresponding control used for this transition is stored in $U(i,k)$. The corresponding extracted energy is stored in $I(i,k)$.

The three matrices (S, U and I) are initialized recursively. Starting from the initial state $\vec{x}_0$ at time t_0, each of the Nu discrete control values between u_{max} and $-u_{max}$ is applied to $\vec{x}_0$ to compute a set of new states $\vec{x}_1, \cdots, \vec{x}_{Nu}$ at time t_1. The associated states ($\vec{x}_{\mathbf{a}0}$, $\vec{x}_{\mathbf{a}l}$, $\cdots$, and $\vec{x}_{\mathbf{a}Nu}$) of the states $\vec{x}_0$, $\vec{x}_1$, $\cdots$, and $\vec{x}_{Nu}$, respectively, are computed and stored in the S matrix.

$$\begin{aligned} S(\vec{x}_{\mathbf{a}l}, 1) &= \vec{x}_{\mathbf{a}0} \\ &\vdots \\ S(\vec{x}_{\mathbf{a}Nu}, 1) &= \vec{x}_{\mathbf{a}0} \end{aligned} \tag{34}$$

The corresponding controls and extracted energies are stored in U and I matrices as follows

$$\begin{aligned} U(\vec{x}_{\mathbf{a}l}, 1) &= u_1 \\ &\vdots \\ U(\vec{x}_{\mathbf{a}Nu}, 1) &= u_{Nu} \\ I(\vec{x}_{\mathbf{a}l}, 1) &= u_1 \times \vec{x}_0(2) \\ &\vdots \\ I(\vec{x}_{\mathbf{a}Nu}, 1) &= u_{Nu} \times \vec{x}_0(2) \end{aligned} \tag{35}$$

Starting from each of $\vec{x}_1, \ldots, \vec{x}_{Nu}$ as initial states, the above process is repeated recursively until time t_N to initialize the three matrices. The extracted energy is accumulated in subsequent steps, e.g.,

$$I(\vec{x}_{\mathbf{a}4}, 2) = I(\vec{x}_{\mathbf{a}1}, 1) - u_1 \times \vec{x}_1(2) \tag{36}$$

After initialization, the last column in the I matrix is scanned for the maximum value (maximum extracted energy). This entry in the I matrix at time t_N is traced back in the U matrix to find the corresponding control at initial time u_1. This initial control is applied to the initial state to compute the new updated state. The above process repeats iteratively. It is not necessary to compute the full matrices anymore; we only need to compute one additional column in each matrix, at each new time step.

3.5. Shape-based (SB) control

The SB approach was recently developed for control of wave energy conversion [25], for space trajectory optimization [26, 27, 28, 29], and it has its roots in pseudo-spectral

optimal control [30, 31]. In pseudo-spectral methods, the system dynamics are approximated by function series. The derivative of the state vector is approximated by the analytic derivative of the corresponding approximating function of the state.

This SB approach differs from the pseudo-spectral optimal control approach in that it approximates only one state (buoy's vertical velocity) using Fourier series as opposed to approximating all the system's states and the control in pseudo-spectral methods; hence the SB method is computationally faster. The SB approach benefits from a priori knowledge about the shape of one of the states to generate a good initial guess for the optimization process. In this development, the buoy's vertical velocity is selected to be the approximated state since the shape of the wave vertical velocity can be used as initial guess for the buoy's vertical velocity. For this, a Fourier series expansion is used for approximation. Hence, existing, well-developed optimization algorithms may be used to solve the transformed problem [31].

The SB control approach is a receding horizon strategy. The implementation of SB used here does not include an inner feedback loop (block $C_{FB}(s) = 1$ and feedback block $H_{FB}(s) = 0$). However, as shown in Figure 5, the current state of the system is passed to the optimization block directly.

For the WEC optimal control problem, the SB control approach approximate the buoy's vertical velocity, $v_f(t)$, as follows:

$$v_f(t) \equiv x_2 = \frac{a_0}{2} + \Sigma_{n=1}^{N} \left(a_n \cos\left(\frac{n\pi}{H} t\right) + b_n \sin\left(\frac{n\pi}{H} t\right) \right) \tag{37}$$

Where H is the predication horizon time interval, and N is number of Fourier terms which is a design parameter. The coefficients a_0, a_n, and b_n are the design variables to be optimized in order to obtain the shape of $v_f(t)$ that would maximize the extracted energy. (Note that including a_0 in (37) allows for a nonzero initial value for $v_f(t)$.) For a given set of the coefficients, $v_f(t)$ is computed using (37). The PTO control input associated with the obtained buoy's vertical velocity is computed using the system's dynamic model (A, B, C, D matrices).

The SB optimal control problem is formulated as: find the optimal values of the coefficients a_0, a_n, and b_n, $\forall\, n = 1 \cdots N$ such that the extracted energy is maximized,

subject to the constraints: $u(t) < u_{max},\ 0 < t < T$. The optimal control problem is converted to a parameters optimization problem. An interior point optimization algorithm is used for optimizing the coefficients. A good initial guess for the coefficients a_0, a_n, and b_n $(\forall\, n = 1 \cdots N)$ can be obtained if we note that the wave velocity model can be approximated using Fourier series as follows:

$$w(t) = \frac{c_0}{2} + \Sigma_{n=1}^{N} \left(c_n \cos\left(\frac{n\pi}{T} t\right) + d_n \sin\left(\frac{n\pi}{T} t\right)\right) \tag{38}$$

In (38), the coefficients c_0, c_n, and d_n can be computed given a prediction for $w(t)$. These coefficients are used as initial guesses for the coefficients a_0, a_n, and b_n, respectively.

The SB approach computes the required control at each control update step over the prediction horizon. These control updates are stored. In order to save computational time, it is possible to use these control updates at subsequent control time steps without updating the control calculations. The number of control steps that do not need control calculations is $CtrlInteg$. The following parameters need to be selected:

- N_H : an integer that represents the horizon length in units of wave period (or peak period for irregular sea states)
- N_{cw} : an integer that determines the number of control updates in one wave period
- N_{FFT} : the number of Fourier terms
- $CtrlInteg$: an integer that determines the step of updating the control calculations

The optimal selection for these parameters varies depending on the sea state being solved. Table 4 shows the parameters' values for some of the irregular sea states.

3.6. Linear quadratic (LQ) control

Linear quadratic (LQ) control is a pure feedback control strategy (see Figure 4), meaning that the control signal can be expressed as a function of the current state by means of the controller $C_{FB}(s)$. For this reason, the LQ control strategy requires a state estimator (block $H_{FB}(s)$). LQ does not include any feedforward block ($C_{FF}(s)$) nor input conditioning/pre-filtering block ($H_{ref}(s)$), and the reference signal r is zero.

LQ optimal control is an optimization based design technique for the calculation of a feedback law. The linear quadratic regulator (LQR) and the linear quadratic Gaussian (LQG) controller are two common "special cases" of LQ optimal control problems. In particular, consider the linear dynamical system (non-necessarily time-invariant)

$$\dot{x}(t) = A(t)x(t) + B(t)u(t), \tag{39}$$

where $u(t) \in \mathbb{R}^m$ is the input and $x(t) \in \mathbb{R}^m$ is the state. The objective of the LQR is to find a feedback matrix $K(t)$, such that the closed-loop system with feedback

$$u(t) = -K(t)\, x(t) \tag{40}$$

minimizes the function J

$$J = \int_{t_0}^{t_f} x^T Q x + x^T\, H\, u + u^T R\, u\; dt + x(t_f)^T\, F\, x(t_f), \tag{41}$$

where $Q \geq 0$, $F \geq 0$ and $R > 0$ [32]. The weight matrices Q, H, R, and F are in general design parameters to be tuned. The feedback gain K is calculated as $K(t) = R^{-1}B^T P(t)$, where the symmetric matrix P is the solution of the Riccati equation

$$-\dot{P} = P\, A + A^T P - (P\, B + H)\, R^{-1} \left(B^T\, P + H^T\right) + Q, \tag{42}$$

with boundary condition $P(t_f) = F$.

A special case of the LQR problem is the infinite-time and time-invariant LQR, that is when $t_f \to \infty$ and the matrices A and B are constant. In this case, both the gain matrix K and the matrix P are constant; in particular,

$$K = R^{-1}B^T P \tag{43}$$

and P is the solution of Continuous time Algebraic Riccati Equation (CARE)

$$P\, A + A^T P - (P\, B + H)\, R^{-1} \left(B^T\, P + H^T\right) + Q. \tag{44}$$

The LQG control problem differs from the LQR in that it considers dynamical systems affected by noise and for which the state is not accessible. The LQG problem is solved by

applying the separation principle, stating that the control design and the estimator design can be carried out independently. In practice, the LQG comprises an LQR and a Kalman filter, which is used for the estimation of the state from noisy outputs (measurements). Assuming the system is time-invariant, it may be described as

$$\dot{x} = Ax + Bu + k \tag{45}$$

$$y = Cx + \varpi, \tag{46}$$

where y is the system output, k is the system noise and ϖ is the measurement noise. A fundamental assumption for optimality is that the noise (both k and ϖ) is white and Gaussian. The estimate of the state $\hat{x}$ is given by the Kalman-Bucy filter

$$\dot{\hat{x}} = A\hat{x} + Bu + L(y - C\hat{x}) \tag{47}$$

with initial condition $\hat{x}(0) = E[x(0)]$. The Kalman gain L is calculated as $L = S\,C^T W^{-1}$ with $W = E[\varpi\,\varpi^T]$. The term S is the solution of the Riccati equation.

$$0 = A\,S + S\,A^T - S\,C^T W^{-1}\,C\,S + V \tag{48}$$

where $V = E[k\,k^T]$. By applying the separation principle, the gain K is calculated as in the LQR case, that is via (43), and by using the same Riccati equation in (44) for the calculation of P.

For this study, both the control system and the estimator are designed based on the formulation described in [7] as a single-input/single-output. However, the LQG allows the design of multi-input/multi-output controllers. More specifically, the controller model is composed of a linear system (A_d, B_d, C_d) describing the heave dynamics, combined with a second linear system (A_e, B_e, C_e) describing the excitation, which is considered as colored system noise. Thus, we write the dynamic model in heave as

$$\dot{x}_d = A_d\,x_d + B_d\,u + B_d\,f_e \tag{49}$$

$$y = C_d x, \tag{50}$$

while the model of the excitation force is

$$\dot{x}_e = A_e\, x_e + B_e\, \varpi \tag{51}$$

$$f_e = C_e\, x_e \tag{52}$$

The state vector x_d and the system matrices A_d and B_d the same as those used in (6) (i,e,. $A_d = A_c$ and $B_d = B_c$). The input u is the PTO force and the output y is the heave velocity ($y = v$), thus the output matrix C_d is different from (6) (i.e., it is the last row of C_c in (6)).

The linear system (A_e, B_e, C_e) is obtained by first approximating the wave spectrum $S(\omega)$ with a transfer function $\tilde{S}(\omega) \approx S(\omega)$, as described in [33]. The spectral characteristics of the sea are assumed to follow a Bretschneider distribution. The excitation force $E(\omega)$ is calculated as

$$E(\omega) = H(\omega)\, \tilde{S}(\omega), \tag{53}$$

where $H(\omega)$ is the excitation FRF defined in (3), and the matrices A_e, B_e, C_e are obtained through a balanced realization of the transfer function $E(\omega)$. The matrices of the augmented state space model are built as

$$A = \begin{bmatrix} A_d & B_d C_e \\ \mathbf{0} & A_e \end{bmatrix} \qquad B' = \begin{bmatrix} B_d \\ \mathbf{0} \end{bmatrix} \qquad B_\varpi = \begin{bmatrix} \mathbf{0} \\ B_e \end{bmatrix} \qquad C' = \begin{bmatrix} C_d & \mathbf{0} \end{bmatrix}, \tag{54}$$

resulting in the dynamical system

$$\dot{x} = A\, x + B'\, u + B_\varpi\, \varpi \tag{55}$$

$$y = C'\, x. \tag{56}$$

The system is analogous to the model for the LQG problem in (45) and (46). However, the cost function to be minimized is different. In fact, the objective is to maximize the expected value of the electrical absorbed power $\bar{P}_{abs} = E[-\nu_{out}\, i]$, where ν_{out} is the output voltage and i is the current. The instantaneous power can be written as

$$-\nu_{out}\, i = -\left(\nu_{emf} + R\, i\right) i = -\nu_{emf}\, i - R\, i^2, \tag{57}$$

where ν_{emf} is the back electromotive force. As depicted in Figure 7, the force and velocity are related to the current and voltage as

$$f = K_i\, i \qquad\qquad \nu = K_v\, v, \tag{58}$$

thus the dynamical system can be redefined in terms of the current i as the input, and the voltage ν_{out} as the output, by redefining B and C as

$$B = B'\, K_i \qquad\qquad C = K_v\, C'. \tag{59}$$

The resulting LQ problem is then defined by the cost function

$$J = -E\left[x^T\, H\, i + i^T\, Ri\right], \tag{60}$$

subject to the dynamical the model

$$\dot{x} = A\, x + B\, i + B_{\varpi}\, \varpi \tag{61}$$

$$v = C\, x. \tag{62}$$

Note that (60) is written in the same form as the standard LQ problem in (41), with $Q = 0$ and $H = C^T$. The R matrix corresponds to the resistance in the PTO model.

The LQ problem defined by (60), (61) and (62) depends of the wave spectra because the matrices A_e, B_e, C_e are calculated from $S(\omega)$. Therefore, the feedback gain, optimized by (60), needs to be updated whenever the spectral properties of the sea change. The optimization problem has an analytical solution (the feedback gain matrix) because the problem is linear quadratic (LQ) (i.e., the model is linear and the cost function is quadratic). The solution to the LQ problem is found by solving the CARE in (44), which is build using (60), (61), and (62). With this control strategy is not possible to include constraints in the problem formulation.

3.7. PD version of CC control (PDC3)

This control strategy sub-optimally (in terms of power absorption) realizes complex conjugate control (CCC) via a feedback strategy (see Figure 4) by creating a resonate

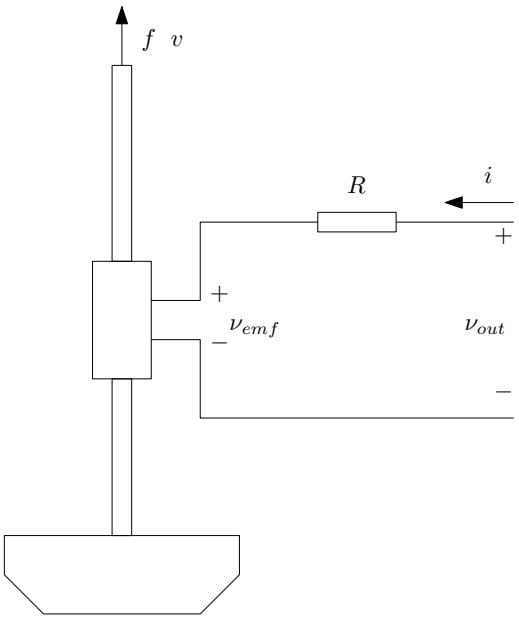

Figure 7: Schematic for LQ control.

generator. The theoretical underpinnings of complex conjugate control are fundamentally linear, and hence PDC3 this is also linear. This strategy targets individual frequency components that come from the excitation input signal. Each individual frequency uses a proportional-derivative (PD) control to provide both optimal resistive and reactive elements. By resonating each frequency component and summing them together, the controller feedback effort that maximizes the amount of absorbed power is provided. A fully detailed description of this control strategy is provided in [34].

The controller model consists of a linear transfer function with individual feedback for a bank of filters that isolate primary frequencies associated with a given sea state irregular wave input profile. Control design consists of an offline filter design optimization process that includes the number of filters and frequencies selected with their corresponding Q-factor (which is a parameter related to the bandwidth of the filter). The optimal P and D are values are derived from linear complex conjugate control. The goal is to have the filters resonate for frequencies that are off-resonance, which will require reactive power to help boost total energy capture width and absorbed power.

In the current implementation, the filter sets are sea state specific. A range of $1-3$

peaking filters where used during this study for each sea state. As development work continues on this strategy, the filter set is expected to become sea state independent.

3.8. Latching

Latching is a type of switching control, the origins of which in wave energy conversion can be traced back to early studies on small heaving point absorber buoys with short natural resonant periods. The technique consisted of locking the buoy displacement until the approach of a crest (or a trough) and releasing it so it achieved full velocity at the crest (or trough) and then re-locking the displacement until the approach of the next crest or trough. A formal theoretical foundation was established in the mid-eighties through the work of Hoskin and Nichols [5]. In practice, the objective of latching control can be seen as to maximize the absorbed power by "keeping" the velocity of the buoy in phase with the excitation force. The strategy is most effective when the incoming wave has a period greater than the resonance period of the oscillating body because by holding the device in a latched state for a given amount of time, the net result can be understood as "shifting" the resonance period of the device to a larger value.

Latching is a mixed feedback/feedforward control strategy, and its implementation is based on the prediction of the excitation force caused by the incident wave. Rather than the exact profile of the excitation force, latching requires the prediction of the next peak in the excitation force. Although the design of the latching control strategy has been based on a single DOF device, it can be also be implemented with additional DOFs (see, e.g., [35]).

Latching is a type of nonlinear control because the control variable can only assume two values, 1 or 0. Typically, latching involves application of resistive loads only, so it is a sub-optimal control in the hydrodynamics sense. The entire formulation is developed in the time domain, and is framed as an optimal switching control problem.

The optimal switching sequence is one that leads to maximum power absorption over a duration of time T, subject to the constraints imposed by the converter dynamic model and limits on PTO force and stroke-length. In the framework of Hoskin and Nichols [5], the switching sequence is derived using the Pontryagin Max/Min principle. Implicit in the procedure, is the need to solve a two-point boundary value problem in the time domain, where the boundary extends from the current instant to T time units into the future.

Therefore, prediction of the exciting force is required even though the control leads to suboptimal velocities. Early latching solutions evaluated the optimal switching sequence using an iterative procedure. More expedient approaches have evolved in recent years, among which empirical rules to calculate the switching sequence [36]. In this case, the device is latched whenever the buoy reaches zero velocity and it is released approximately $T_{res}/4\,\mathrm{s}$ before the next predicted peak in the excitation force, where T_{res} is the resonance period of the device.

The calculation of the latching control law can be carried out online in both the Hoskin and Nichols [5] approach, where the implementation is based on Pontryagin Max/Min principle, and in the empirical approach [36]. The Hoskin and Nichols approach, however, may not be suitable for real-time implementation due to the required intensive computation. On the opposite side, the empirical approach requires the prediction of the incoming excitation force and the resonance period of the device (T_{res})[1], but it is generally suitable for real-time implementation.

Latching is a type of switching control (Figure 8), the implementation of which is carried out by assuming that the force exerted by the linear generator is of the form

$$f_u = -(B_u + u(t)\,B_L)v(t) \tag{63}$$

where v is the heave velocity of the buoy and B_u is the damping coefficient used for power absorption, such that the instantaneous absorbed power is $P_u(t) = -f_u(t)\,v(t) = B_u\,v(t)^2$. The control signal $u(t)$ is a switching binary function that takes the value of 0 when the device in unlatched (absorption mode), or 1 when the device is latched. When the device is in latched mode $(u(t) = 1)$, then the total of the damping exerted by the PTO is equal to $B_u + B_L$, where, in practice, B_L takes a value large enough to prevent the device from moving. However, since the value of B_L is not infinite, the device moves with a very small velocity when latched.

The optimal switching policy for $u(t)$ can be obtained by using Pontryagin principle [5]; however, this approach is not suitable for real-time implementation because of the high computational cost. The solution chosen for the switching policy is the empirical

[1] The resonance period is fixed once the structural/hydrodynamical properties of the device have been set.

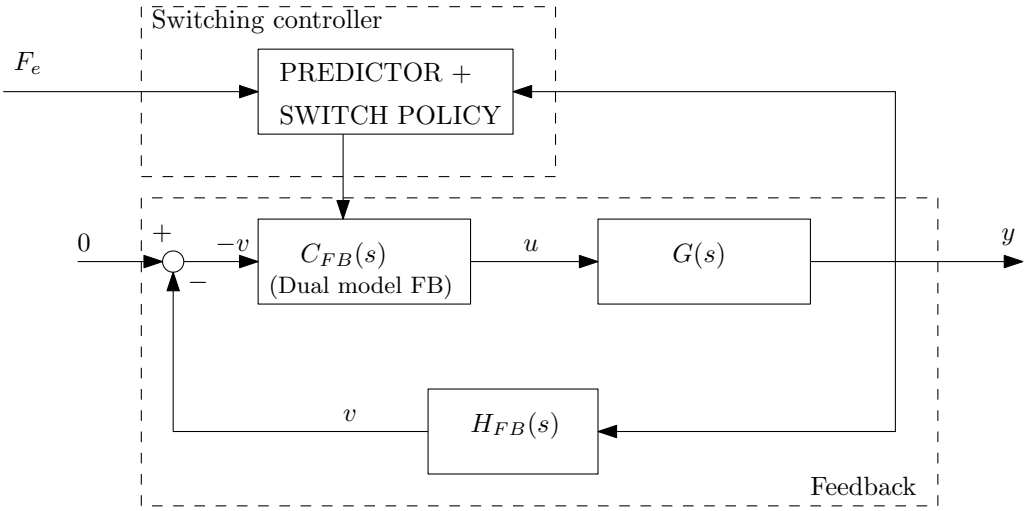

Figure 8: Structure of latching control.

method described by Budal and Falnes in [36], where the device is being latched whenever it reaches zero velocity, and it is being released a quarter of the resonance period before the next predicted peak in the excitation force. Figure 9 illustrates the working principle of latching control: by holding the device locked for an appropriate time interval so as the peak of the velocity matched with the peak of the excitation force, the oscillating body moves at considerably higher peak velocity and it absorbs more power.

4. Results & discussion

Table 5 summarizes the relative performance of the assessed control strategies in irregular waves. Six different quantities are considered: net power, reactive power, PTO force, position, velocity, and acceleration. Here, net power is the absorbed power minus any reactive power (note that this does not include any consideration for efficiency, i.e., the motor is considered to be 100% efficient). Reactive power is power expended by the WEC. For each of these quantities, three different statistical measures are reported: average (mean), peak (98th percentile), and ratio of peak over average. For the averages, the reported value is obtained based on an average annual calculation, which takes into account the relative occurrence of the sea states analyzed. All values are given as the average annual value for the quantity defined. Further, all units are metric and all results

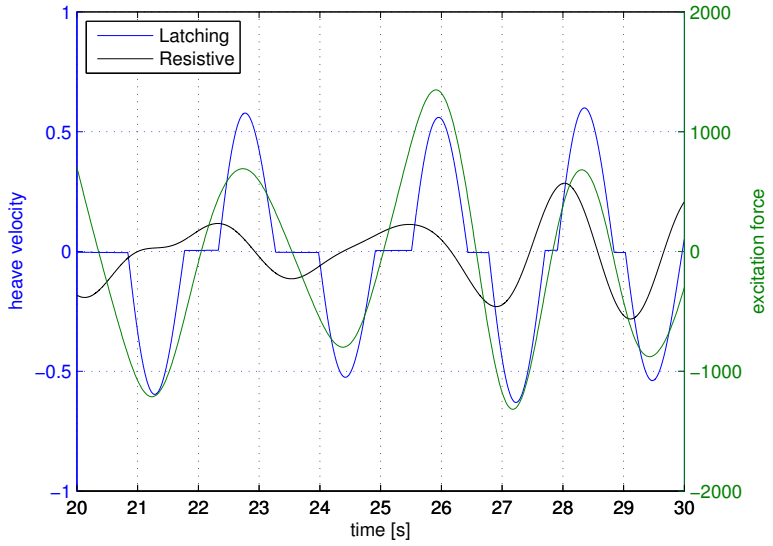

Figure 9: Heave velocities of latching control versus resistive control.

are shown in model scale.

From Table 5, we can see that the various control strategies have a wide range of performances. For example, the average net power produced ranges from 52.5 W for CCC to 15.5 W for resistive control. While CCC is not considered directly implementable, MPC produced nearly as much net power with 46.1 W (roughly 3 times that of resistive control). PDC3, LQ, and Latching control, which are all purely feedback, produce similar levels of net power (on the order of 25 W).

The peak/average net power also shows a wide range of results. This metric is considered to be somewhat similar to a capacity factor, in that it might indicate the degree to which a WEC design utilizes its capabilities. A lower peak/average net power ratio would mean that the device is generally operating in a similar region, avoiding the need for components (e.g., PTO and power electronics) to be over-designed to accommodate infrequent spikes. LQ shows good power absorption (50% more than resistive control), while maintaining a low peak/average net power ratio. Conversely, PDC3 shows a relative large peak/average net power ratio. This may be partially due to some tuning, which could be improved reduce spikes in absorption.

Many of the strategies utilize reactive power levels an order of magnitude greater

than the net absorbed power. This may prove unrealistic in physical implementation, as the PTO would need to be sized quite large to supply the necessary reactive power. LQ also uses orders magnitude less reactive power compared to some of the other strategies. This may be partially due to the fact that LQ is the only strategy that includes a model, although very simplistic, of the PTO, which includes a resistor that provides a basic, lumped parameter, linear model for the PTO inefficiency.

As with other metrics considered here, PTO forces required by the different control strategies span a full order of magnitude. However, the peak/average force ratios from each strategy were relatively similar (much more so than the net power peak/average ratios). Acceleration may serve as a rough proxy for the loading on the mechanical/structural components of a device. LQ has the lowest acceleration in Table 5; while DP and CCC have the highest. Not surprisingly, latching control also tends to produce relatively large accelerations.

It is also somewhat useful to compare the time history responses of the different control strategies. Figure 10a shows a sample time-history from select control strategies for the irregular sea state 15 ($H_s = 0.32\,\mathrm{m}$, $T_p = 3.6\,\mathrm{s}$). The four subplots (a-d) show the heave velocity, heave position, PTO force and instantaneous absorbed power, respectively. For each of the subplots, the excitation force (which is fully linear and therefore the same for each of the control strategies) is shown in green.

It is interesting to note that all the control strategies attempt to improve the "phase matching" between velocity and excitation force, when compared to resistive control. The plots also show the different specific method each control strategy uses to keep velocity in phase with excitation. Latching control locks the device in order to match the peaks of the velocity with the peaks of the excitation force. MPC and LQ force the device to follow excitation with a smoother profile, by using reactive power (Figure 10d), that is by accelerating the device by means of the actuator force. The smoother motion resulting from MPC and LQ can be observed also by looking at the time profiles of the position (Figure 10b) and the force exerted by the actuator (Figures 10c).

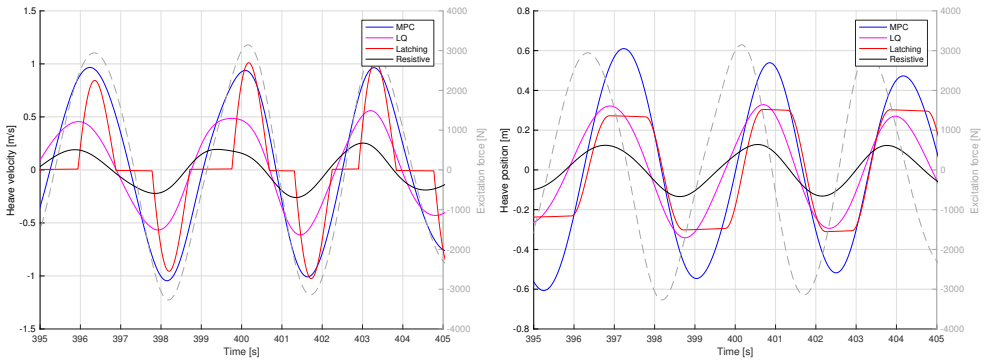

(a) Heave velocity

(b) Heave position

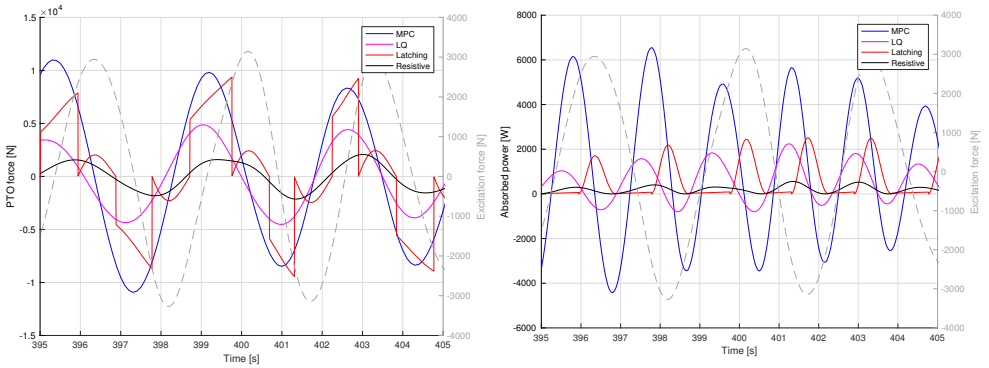

(c) PTO force

(d) Instantaneous power

Figure 10: Sample time histories from irregular sea state 15 ($H_s = 0.32\,\mathrm{m}$, $T_p = 3.6\,\mathrm{s}$).

5. Conclusions

This study considered and evaluated a series of eight WEC control strategies. In addition to strategies well-studied for WECs, some novel strategies for this application were also introduced. Using a numerical simulation, each strategy was utilized to simulate the WEC response in a series irregular sea states. The results from these simulations were distilled to provide a concise comparison of the performance produced by the different control strategies. In addition to the obvious metric of power absorption, other performance metrics were studied with the aim of providing some insight into the relative costs and challenges of implementing the different control strategies. As WECs are intended to be commercially profitable devices, this type of consideration is essential.

The results shown in this study begin to highlight the need for a holistic approach to WEC design. So-called "co-design" practices, where components of a system design which are often taken into account sequentially are instead considered in conjunction with each other, will be needed to properly utilize advanced control for a WEC. Fundamental design factors, such as the characteristic scale of a WEC, cannot properly be considered without considering in earnest the eventual control strategies which may be implemented on the device.

Thus, future work should consider a more comprehensive assessment of how control design interfaces with overall WEC design. In this study, a device with a fixed design was augmented with a series of control strategies. However, a more realistic study would consider control design as part of the larger WEC design process. Also, some additional development on the formulation of performance metrics would be helpful. Instead of simply considering, for example, the peak PTO force across a series of sea states, processes defined by design standards and technical specifications should be followed. In addition to peak loading, modeling for fatigue could provide an important consideration.

If possible, similar studies should also be conducted for different WEC devices. This study presents results only for a single specific device. We believe that the results provide some general relative comparison, but further work will be necessary to establish just how much such a comparison will vary for different device designs and archetypes. Additionally some further understanding can be obtained by considering control performance in regular waves, and by normalizing both regular and irregular wave results with respect

to the natural frequency of the device.

It will also be useful to consider a more complete model of the WEC system. As is typical, only the hydro-mechanical system is considered in this study. Mechanical power is used as a performance metric, but most WEC systems are targeted at producing electricity. Thus the PTO and power electronics should be considered to provide a fuller assessment. By adding these components for both plant and control models, the impact of generator efficiencies and dynamics can be included in the comparison. This may, for example, tend to penalize strategies which use large amounts of reactive power. In this study, the only strategy to somehow take into account some aspects of the PTO efficiency is LQ control, which includes a model of the internal resistance of the generator circuit. Another consideration, highlighted by the large levels of peak reactive utilized by many of the strategies considered here, would be to apply constraints to curtail reactive power levels.

A related ongoing project is focused on PTO design, considering integration with the full WEC system, grid, and control. The purview of this work includes consideration for stored energy in order to provide both reactive power and smoothing. Since the PTO may indeed play an important role in the overall system dynamics, it is possible that including this in the plant for control design could greatly affect outcome of a study such as this.

Another important factor not fully considered here is the realistic implementation of these various control strategies on a deployed device. For this study, the control model is considered to be perfectly accurate (i.e. the control model and plan model are the same). However, this will certainly not be the case in implementation. Model uncertainties and nonlinearities not captured by the reduced-order control model are likely to adversely affect the performance of controllers. The magnitude of such adverse effects will be dependent on the specific control strategy. Additionally, this study assumed perfect foreknowledge of incoming waves and no sensor noise. While methods are available for filtering noisy measurement signals and estimating/predicting the system state, limitations in these methods, and their affect on controller performance should be considered in future studies.

Acknowledgements

This work was funded by the U.S. Department of Energy's Wind and Water Power Technologies Office. Sandia National Laboratories is a multi-mission laboratory managed and operated by National Technology and Engineering Solutions of Sandia, LLC., a wholly owned subsidiary of Honeywell International, Inc., for the U.S. Department of Energys National Nuclear Security Administration under contract DE-NA0003525.

References

[1] K. Budal, J. Falnes, Interacting point absorbers with controlled motion, in: B. Count (Ed.), Power from Sea Waves, Academic Press London, Edinburgh, Scotland, 1979, pp. 381–399.

[2] D. Jones, Wave energy conversion, Patent: US 4355511 A (1977).

[3] D. V. Evans, A theory for wave-power absorption by oscillating bodies, Journal of Fluid Mechanics 77 (01) (1976) 1–25. doi:10.1017/S0022112076001109.
URL http://journals.cambridge.org/action/displayAbstract?fromPage=online&aid=374123

[4] L. C. Iversen, Numerical method for computing the power absorbed by a phase-controlled point absorber, Applied Ocean Research 4 (3) (1982) 173–180.

[5] R. Hoskin, B. Count, N. Nichols, D. Nicol, Phase control for the oscillating water column, in: D. Evans, A. de Falco (Eds.), Hydrodynamics of Ocean Wave-Energy Utilization, International Union of Theoretical and Applied Mechanics, Springer Berlin Heidelberg, 1986, pp. 257–268. doi:10.1007/978-3-642-82666-5_22.
URL http://dx.doi.org/10.1007/978-3-642-82666-5_22

[6] A. Babarit, A. Clement, Optimal latching control of a wave energy device in regular and irregular waves, Applied Ocean Research 28 (2) (2006) 77–91. doi:10.1016/j.apor.2006.05.002.
URL http://www.sciencedirect.com/science/article/pii/S0141118706000423

[7] J. T. Scruggs, S. M. Lattanzio, A. A. Taflanidis, I. L. Cassidy, Optimal causal control of a wave energy converter in a random sea, Applied Ocean Research 42 (2013) 1–15. doi:10.1016/j.apor.2013.03.004.
URL http://www.sciencedirect.com/science/article/pii/S0141118713000205

[8] J. A. M. Cretel, G. Lightbody, G. P. Thomas, A. W. Lewis, Maximisation of energy capture by a wave-energy point absorber using model predictive control, in: IFAC World Congress, 2011.

[9] G. Li, M. R. Belmont, Model predictive control of a sea wave energy converter: a convex approach, in: 19th World Congress of the International Federation of Automatic Control, Cape Town, South Africa, 2014.

[10] J. Hals, J. Falnes, T. Moan, A comparison of selected strategies for adaptive control of wave energy converters, Journal of Offshore Mechanics and Arctic Engineering 133 (3) (2011) 031101. doi:10.1115/1.4002735.

URL http://offshoremechanics.asmedigitalcollection.asme.org/article.aspx?articleid=1456895

[11] R. G. Coe, G. Bacelli, D. Patterson, D. G. Wilson, Advanced WEC Dynamics & Controls FY16 testing report, Tech. Rep. SAND2016-10094, Sandia National Labs, Albuquerque, NM (October 2016).
URL https://mhkdr.openei.org/submissions/151

[12] W. E. Cummins, The impulse response function and ship motions, Tech. Rep. DTNSDRC 1661, Department of the Navy, David Taylor Model Basin, Bethesda, MD (1962).
URL http://dome.mit.edu/handle/1721.3/49049

[13] T. Burton, Volterra Integral and Differential Equations, Elsevier, 2005.
URL http://www.sciencedirect.com/science/bookseries/00765392/202

[14] T. Perez, T. I. Fossen, Time- vs. frequency-domain identification of parametric radiation force models for marine structures at zero speed, Modeling, Identification and Control 29 (1) (2008) 1–19. doi:10.4173/mic.2008.1.1.
URL http://www.mic-journal.no/PDF/2008/MIC-2008-1-1.pdf

[15] R. G. Coe, D. L. Bull, Nonlinear time-domain performance model for a wave energy converter in three dimensions, in: OCEANS2014, IEEE, St. John's, Canada, 2014.

[16] WAMIT, WAMIT User Manual, Chestnut Hill, MA, 7th Edition (2012).
URL http://www.wamit.com/manual.htm

[17] G. Bacelli, R. G. Coe, D. Patterson, D. Wilson, System identification of a heaving point absorber: Design of experiment and device modeling, Energies 10 (10) (2017) 472. doi:10.3390/en10040472.
URL http://www.mdpi.com/1996-1073/10/4/472

[18] J. Lavelle, J. P. Kofoed, Representative spectra of the wave resource from sea wave measurements, in: European Wave and Tidal Energy Conference (EWTEC), Aalborg, Denmark, 2013.
URL http://www.researchgate.net/profile/John_Lavelle2/publication/267763888_Representative_Spectra_of_the_Wave_Resource_from_Real_Sea_Wave_Measurements/links/545a287b0cf2cf51648437dc.pdf

[19] K. Aström, R. Murray, Feedback Systems: An Introduction for Scientists and Engineers, Princeton University Press, 2010.

[20] K. Ogata, Modern Control Engineering, Prentice Hall, 2002.

[21] J. Falnes, Ocean Waves and Oscillating Systems, Cambridge University Press, Cambridge; New York, 2002.

[22] J. Falnes, On non-causal impulse response functions related to propagating water waves, Applied Ocean Research 17 (6) (1995) 379–389. doi:10.1016/S0141-1187(96)00007-7.
URL http://www.sciencedirect.com/science/article/pii/S0141118796000077

[23] D. P. Bertsekas, Dynamic Programming and Optimal Control, 4th Edition, Athena Scientific, 2012.

[24] R. D. Robinett, Applied dynamic programming for optimization of dynamical systems, Society for Industrial and Applied Mathematics, Philadelphia, 2005.

[25] O. Abdelkhalik, R. Robinett, S. Zou, G. Bacelli, R. Coe, D. Bull, D. Wilson, U. Korde, On the

control design of wave energy converters with wave prediction, Journal of Ocean Engineering and Marine Energy 2 (4) (2016) 473–483. doi:10.1007/s40722-016-0048-4.
URL http://dx.doi.org/10.1007/s40722-016-0048-4

[26] E. Taheri, O. Abdelkhalik, Approximation of constraint low thrust space trajectories using Fourier series, in: AAS / AIAA Astrodynamics Specialist Conference, no. AAS11-555, Girdwood, Alaska, USA, 2011.

[27] E. Taheri, O. Abdelkhalik, Shape based approximation of constrained low-thrust space trajectories using Fourier series, Journal of Spacecraft and Rockets 49 (3).

[28] O. Abdelkhalik, E. Taheri, Approximate on-off low-thrust space trajectories using Fourier series, Journal of Spacecraft and Rockets, AIAA 49 (5) (2012) 962–965.

[29] E. Taheri, O. Abdelkhalik, Constraint low-thrust trajectory planning in three-body dynamic models: Fourier series approach, in: AIAA Space and Astronautics Forum and Exposition, AAS / AIAA Astrodynamics Specialist Conference, no. AIAA-2014-4464, San Diego, CA, USA, 2014.

[30] I. M. Ross, M. Karpenko, A review of pseudospectral optimal control: From theory to flight, Annual Reviews in Control 36 (2) (2012) 182 – 197. doi:http://dx.doi.org/10.1016/j.arcontrol.2012.09.002.
URL http://www.sciencedirect.com/science/article/pii/S1367578812000375

[31] G. Elnagar, M. Kazemi, M. Razzaghi, The pseudospectral legendre method for discretizing optimal control problems, Automatic Control, IEEE Transactions on 40 (10) (1995) 1793–1796. doi:10.1109/9.467672.

[32] B. D. Anderson, J. B. Moore, Optimal Control - Linear Quadratic Methods, Prentice-Hall International, Inc., 1989.

[33] P.-T. Spanos, Filter approaches to wave kinematics approximation, Applied Ocean Research 8 (1) (1986) 2 – 7. doi:http://dx.doi.org/10.1016/S0141-1187(86)80025-6.
URL http://www.sciencedirect.com/science/article/pii/S0141118786800256

[34] D. Wilson, G. Bacelli, R. D. Robinett III, U. Korde, O. Abdelkhalik, S. F. Glover, Order of magnitude power increase from multi-resonance wave energy converters, in: OCEANS 2016 MTS/IEEE Monterey, 2017.

[35] A. F. O. Falcao, P. A. Justino, J. C. Henriques, J. M. Andre, Reactive versus latching phase control of a two-body heaving wave energy converter, in: European Control Conference (ECC), 2009, pp. 3731–3736.

[36] K. Budal, J. Falnes, T. Hals, L. C. Iversen, T. Onshus, Model experiment with a phase controlled point absorber, in: Proc. of the Second International Symposium on Wave and Tidal Energy, H. S. Stephens and C. A. Stapleton, eds, BHRA Fluid Engineering (Cranford, Bedford), Cambridge, UK, 1981, pp. 191–206.

Table 2: Full list of the 17 irregular sea states considered in study. Note that sea states listed with an occurrence percentage of 0 are from the constant-steepness set and are not considered for average annual statistics.

Sea State index	**Peak period,** T_p **[s]**	**Significant wave height,** H_s **[m]**	**Steepness,** $(\frac{\lambda_p}{H_s})$ **[-]**	**Occurrence [%]**
1	1.00	0.0247	63	0
2	1.00	0.0148	105	0
3	1.00	0.0370	42	0
4	1.53	0.0871	42	18.5
5	2.00	0.0594	105	0
6	2.05	0.1039	63	17.2
7	2.25	0.1875	42	11.3
8	2.50	0.1545	63	0
9	2.50	0.0927	105	0
10	2.58	0.1194	87	21.1
11	2.89	0.2523	52	7.6
12	3.00	0.3337	42	0
13	3.03	0.1363	105	12.8
14	3.46	0.1283	146	9.2
15	3.60	0.3195	63	4.9
16	4.02	0.1320	191	5.8
17	4.86	0.1617	228	1.6

Table 3: Control strategies evaluated. *categorization is determined based on implementation in this study, however, these strategies can be implemented, e.g., to avoid reactive power.

	Computational expense	**Constraints**	**Reactive**	**Foreknowledge**
Resistive	low	yes	no	no
MPC	moderate-high	yes	yes*	yes
DP	high	yes	yes*	yes
SB	high	yes	yes*	yes
LQ	low	no	yes	no
PDC3	low	no	yes	no
Latching	low	no	no	yes*

Table 4: Selected SB parameters for some of the irregular sea states.

	N_H	N_{cw}	N_{FFT}	$CtrlInteg$
IS10	3	60	7	3
IS11	3	60	6	3
IS12	3	50	7	2
IS13	3	50	8	2
IS14	3	50	7	2
IS15	3	50	7	2
IS16	3	50	7	2
IS17	3	60	7	2

Table 5: Comparison of WEC control strategy performance.

	CCC	**DP**	**LQ**	**Latch.**	**MPC**	**PDC3**	**Res.**	**SB**
Net power [W]								
average	52.5	38.4	23.5	28.8	46.1	26.8	15.5	17.7
peak	4.8E3	4.6E3	4.5E2	3.9E2	1.8E3	1.3E3	1.7E2	4.9E2
peak/average	92.0	119.1	18.9	13.6	38.6	48.4	10.8	27.9
Reactive power [W]								
average	1.3E2	1.7E2	3.7E0	0	4.3E1	3.2E1	0	1.3E1
peak	2.7E3	3.1E3	7.4E1	0	7.6E2	6.8E2	0	1.9E2
peak/average	20.4	18.1	19.7	0	17.8	21.0	0	15.3
PTO force [N]								
average	1.3E3	1.6E3	2.6E2	5.1E2	7.7E2	6.9E2	2.1E2	3.4E2
peak	1.0E4	1.2E4	2.1E3	3.6E3	5.7E3	5.4E3	1.1E3	1.8E3
peak/average	8.1	7.7	8.0	7.2	7.5	7.7	5.0	5.1
Position [m]								
average	7.3E-2	8.4E-2	2.9E-2	3.3E-2	4.9E-2	4.0E-2	1.6E-2	3.0E-2
peak	5.3E-1	5.3E-1	1.6E-1	1.7E-1	3.1E-1	2.8E-1	7.5E-2	1.7E-1
peak/average	7.2	6.3	5.4	5.2	6.4	7.1	4.6	5.7
Velocity [m/s]								
average	1.4E-1	1.5E-1	7.1E-2	6.0E-2	1.0E-1	7.6E-2	4.0E-2	8.7E-2
peak	8.0E-1	8.3E-1	3.1E-1	4.0E-1	5.2E-1	4.1E-1	1.6E-1	4.8E-1
peak/average	5.8	5.5	4.4	6.7	5.1	5.4	4.0	5.5
Acceleration [m/s^2]								
average	0.31	0.38	0.07	0.21	0.13	0.12	0.11	0.28
peak	1.42	1.83	0.31	1.37	0.83	0.58	0.40	1.46
peak/average	4.5	4.9	4.4	6.6	6.2	4.7	3.6	5.3